Phase-Change Heat Regenerators: Modeling and Experimental Studies

Henry F. Erk and M. P. Duduković
Chemical Reaction Engineering Lab., Dept. of Chemical Engineering, Washington Univ., St. Louis, MO 63130

Modeling of and experiments with heat storage in regenerators packed with phase-change material (PCM) are discussed, as well as the second-law thermodynamic efficiency for the ideal phase-change regenerator (PCR). An algorithm to solve the coupled partial differential equations for heat transfer and storage in the PCR on the bed scale and on the PCM scale is presented. The bed is discretized via the tanks-in-series approximation. The PCM scale is solved by orthogonal collocation applied to the equations, transformed to immobilize the melt/solid interface and eliminate the effect of spherical geometry. Parametric studies show the effects of specific dimensionless groups. A novel PCM consisting of n-octadecane retained by capillary forces in a porous silica support is used in a lab-scale PCR to verify the model. It visually changes from opaque to semi-transparent when the wax melts, thereby allowing the melt front within the bed to be tracked. Experiments with heated or cooled CO_2 passing through the PCR are described. The measured outlet temperature compares qualitatively with model predictions. The model quantitatively predicts melt front movement in the first 60% of the bed. Discrepancies between the model and experiments are linked to significant heat losses.

Introduction

Fixed-bed heat regenerators are used to recover, store and reuse waste energy. Large regenerators are used to recover waste heat from power and steam plants and incinerators (Duduković and Ramachandran, 1987; Schmidt and Willmott, 1981; Hausen, 1983; Reiter, 1983; Reay, 1979). These regenerators are cycled between heat storing and heat releasing modes. First, a stream containing waste heat (e.g., exhaust gas from a boiler or incinerator) is passed through the bed where the heat is transferred to the inert packing. Later a cold stream (e.g., the feed air to the boiler or incinerator) is passed through the hot bed thereby heating the stream. Conventional regenerators utilize the sensible heat of the packing to absorb and store energy.

It has long been recognized that compared to sensible heat storage, larger amounts of energy per unit volume can be stored by utilizing the latent heat of a phase change. Energy storage schemes utilizing latent heat of fusion (and solid-state transitions) are the most practical because the change in specific volume for most solid-liquid phase transitions is minimal, thereby eliminating the need for using high-pressure equipment, as would be the case for a scheme utilizing the latent heat of vaporization. For example, the solid-to-liquid phase change of Glauber's salt (Na_2SO_4) was proposed as a store of solar energy for domestic heating (Fellague and Jesh, 1987). In this case, during the daytime hours the incident sunlight shining onto a building is stored as the salt melts. Then at nighttime, as the salt solidified, the released energy can heat the building. Recently, latent-heat "cold-storage" has been proposed as a means of leveling air conditioning loads in hot climates (Electric Power Research Institute, 1987). Still other applications utilizing latent heat storage have been proposed. One scheme, which is being commercialized, uses latent heat to store waste heat from an automobile engine so that it may be used to rewarm the engine in cold climates following being off for more than several hours (Schatz, 1991). This minimizes the period of time the engine is warming, a period of time when fuel efficiency is low and tailpipe hydrocarbon emissions are the highest. A large-scale latent heat store has been proposed for reclaiming high temperature waste energy in the firing of bricks (Adebiyi, 1988).

It is evident that in a typical packed-bed regenerator, far greater amounts of energy can be stored if the packing were replaced with a material which changed phase and stored en-

Current address of H. F. Erk: MEMC Electronic Materials, Inc., St. Peters, MO 63376.

ergy as latent heat. In this case, the heat storage medium is referred to as a phase-change material (PCM). Generally, some means of containing or supporting the PCM must be provided since the material can flow when it is in the liquid state. Two approaches are commonly used: a supported PCM and an encapsulated PCM. With a supported PCM, the liquid phase-change compound is absorbed in an inert porous structure. With an encapsulated PCM, the liquid is contained in a shell of inert material. For either case, some engineering is required to minimize the stress of the support or shell with the change in specific volume as the material changes phase.

A regenerator which utilizes phase-change heat storage is referred to as a phase-change regenerator (PCR). Despite the recent interest in the PCR, there has been a lack of detailed modeling and experimental model verification for this device. Models for the PCR are complex, involving the solution of the classical Stefan problem for phase-change heat storage on the scale of the PCM, coupled with the heat balance equation for the scale of the PCR packed bed. Solutions of models incorporating the nonlinearities introduced by the coupling of these two scales can be utilized in other applications as well, such as gas absorption and/or reaction with solids in packed beds. In this article we describe a detailed model for the PCR and compare the results with experimental data obtained from a lab-scale PCR.

Experimental Studies

Studies on phase-change heat storage have been conducted in many different areas. The scope of this work ranges from single-element heat storage modules to heat storage slurries and PCRs. Here we review only those studies dealing with the PCR itself, i.e., a fixed bed which is packed with PCM.

Wood, Gladwell, O'Callaghan, and Probert (1981) developed a numerical model for the PCR which is packed with an encapsulated PCM. The PCM is assumed to have infinite thermal conductivity: there are no temperature gradients within the PCM. The phase-change process is modeled using the modified heat capacity technique (Shamsundar and Sparrow, 1975). The results are presented as the dimensionless fluid temperature leaving the PCR as a function of dimensionless time, i.e., the dimensionless thermal step-response curves with the number of transfer units (NTU) as a parameter. Wood et al. (1981) show neither their model equations nor describe how the equations are numerically solved. Moreover, the results from the simulations are suspect because the total amount of nondimensional energy which can be stored appears to be a function of NTU, i.e., film-convection heat-transfer coefficient (cf. individual curves of Figure 4 in Wood et al. (1981), note that the area above the step-response curves in this figure is equal to the nondimensional energy stored and this area varies for different values of NTU). Wood et al. also present some experimental results for a PCR packed with 0.02-m-dia. polyethylene spheres filled with a paraffin. Their experimental data indicate a substantial resistance to heat transfer within the PCM, and Wood et al. argue that this gradient is due to water side film resistance. However, the contribution to the overall heat-transfer coefficient due to conductive heat transfer through the 0.001-m-thick polyethylene shell is within 31% of their estimated upper limit for the film coefficient. It is more likely that the heat transfer through the PCM wall was significantly affecting the overall heat-transfer process.

Bell et al. (1982) have discussed the use of a PCR for solar energy heat storage. They performed experiments and developed a model to predict the performance of the PCR filled with a PCM composed of stabilized $Na_2S_2O_3 \cdot 5H_2O$ encapsulated in standard food storage tin cans. No details of their computer model are given. Manley and Smith (1983) have summarized the Bell et al. model simulations. The predicted thermal step-response curve such as the one shown in Figure 6 of Manley and Smith (1983) exhibits a region of isothermal heat storage at a temperature above the melting point of the PCM, which is physically incorrect. The duration of isothermal storage increases as the heat-transfer resistance within the PCR increases, i.e., as NTU decreases. This behavior may be an artifact of the model, since heat storage is no longer isothermal as the NTU decreases. Bell et al. fit their model to their experimental data to estimate the film heat-transfer coefficient. The data indicate that the PCM is considerably supercooled, which was not incorporated in the model.

Arimilli and Graves (1984) and Graves (1985) present experimental studies using a PCR in which a freon is used as the working fluid; thus, phase change takes place in both the PCM and in the surrounding fluid. The PCM was made by encapsulating pelletized Glauber's salt with an organic resin which remained flexible after curing, so the PCM could expand and contract to compensate for density changes. No model for this system is presented.

Arimilli (1987) presents calculations for a PCR filled with spherical PCM. A supported PCM is modeled, composed of a porous matrix filled with a phase-change alloy. The model presented accounts for convection, heat accumulation in the fluid, heat losses through the wall of the PCR, and energy storage by PCM. The model assumes that there are no radial temperature gradients, yet a wall heat loss term is included. The coupled equations for the Stefan problem (PCM-scale) and the bed scale are solved by an iterative finite difference scheme. Results are reported for only a single case: heat recovery from combustion gases. No parametric studies are reported.

Adebiyi (1988) presents a model for a PCR filled with cylindrically-shaped PCM. The PCM cylinders are assumed to be spheres of an equivalent diameter and the enthalpy method (Shamsundar and Sparrow, 1975) is used in solving the model equations. Specific details of how the equations are solved are not given. Only a few results are presented for a specific application: heat storage in the manufacture of bricks. Parametric studies are not presented. A second law efficiency analysis for the PCR is made. A conclusion of this analysis is that the efficiency of the PCR may be maximized if many PCMs, each with a different melting temperature, were used (instead of a PCM which melts at a single temperature) to capture all the different grades of heat energy.

Chen and Yue (1991) have investigated cold storage in a PCR which is packed with porous spheres holding water. They developed a lumped parameter model which assumes the PCR is in a pseudo steady state, which changes as ice is formed. The PCR is depicted as a single, well-stirred tank; dispersion in the bed and heat conduction within the PCM are neglected. Experiments are performed using a 0.1-m-dia.

by 0.260-m-long bed packed with 0.034-mm-OD spheres. The film heat-transfer coefficient was estimated by fitting the model to the experimental data. The model compared favorably with experimental data only with latent-heat storage and badly underpredicted the fluid-outlet temperature when storage was by sensible heat only. Chen and Yue argue that the reason for this discrepancy is that their model assumes a constant film heat-transfer coefficient, when in fact the film coefficient is not constant. However, their data indicate that the assumption of a single stirred tank is not valid. Figure 4 (Chen and Yue, 1991) shows a plot of the temperature distribution at different positions within their experimental PCR. The dimensionless temperature changes by a factor of five between the inlet and outlet of the bed. Since the model is force-fitted to match the outlet temperature by estimating a value of the heat-transfer coefficient, at times when the gradient within the bed is constant (during latent-heat storage) the lumped-parameter model predicts the data trend. When the gradient within the bed changes (as during sensible-heat storage) the model cannot predict the data trend.

Lim et al. (1992) have conducted a second law analysis of phase-change energy storage using multiple PCMs, each melting at a different temperature. Their analysis indicates that for two different PCM, there is an optimal phase-change temperature for each material and ideally the PCM with the highest melting temperature should be packed in the PCR so that it contacts the fluid at the highest temperature. Lim et al. also considered the case where the fluid contacts an infinite number of PCMs. The optimal efficiency is obtained when the melting temperature varies, axially through the bed, as the square root of the fluid temperature. In addition, Lim et al. show that this optimally-efficient arrangement is equivalent to another where there is a single PCM which melts at T_{opt}, where

$$T_{\text{opt}} = (T_{i,h}\, T_0)^{1/2} \tag{1}$$

In Eq. 1, $T_{i,h}$ is the hot fluid temperature at the inlet and T_0 is the reference temperature (i.e., the lowest usable temperature in the sense of the second-law analysis). This result is based upon the assumption there is no backmixing of the hot fluid stream.

The above literature survey indicates that the ideal PCR has not yet been rigorously defined and that the operation of a real PCR has not been modeled in detail. Such a model is needed in order to properly assess the effect of the design and operating parameters on PCR performance. This is the objective of our study.

PCR Model

The information obtainable from a good PCR model consists of: (1) the thermal efficiency; (2) the temperature-time history of the outlet fluid; (3) the thermal breakthrough time; (4) the temperature profile through the bed; (5) the amount of energy stored; (6) temperature profile within an individual PCM at a selected location; and (7) position of the solid-liquid interface within a PCM.

Before presenting the specific details of the model, the ideal case will be considered, which sets the benchmark for estimating the thermal efficiency of the PCR.

Ideal PCR Thermal Efficiency

The ideal PCR is the one in which all heat transfer and storage occur instantaneously, so only bulk convection through the bed is significant. The ideal PCR operates at the highest possible thermal efficiency. The complete development of the behavior for the ideal PCR is presented elsewhere (Erk, 1992), so only the final results will be given here.

Figure 1 gives the step-up and step-down temperature response curves for the ideal PCR. The symbols $T_{i,h}$, $T_{i,c}$, and T_M represent the inlet fluid temperature during the heating (energy storing) period, the inlet fluid temperature during the cooling (energy releasing) period, and the melting temperature of the PCM, respectively. From Figure 1 one observes that the effect of latent heat is to produce two temperature fronts in the bed. The first front with breakthrough time of $\mu_{s,h}$ (heating period) and $\mu_{s,c}$ (cooling period) is analogous to the single front in an ideal conventional (sensible heat storage) regenerator. The only difference between the PCR and conventional regenerator is that for the PCR, the height of the step is limited to T_M. The second front with breakthrough times of $\mu_{l,h}$ (heating period) and $\mu_{l,c}$ (cooling period) represents the effect of latent heat storage. The breakthrough times are given by

$$\mu_{s,h} = \mu_{s,l} = (1+\psi)\frac{L\psi}{v_f \epsilon_B} \tag{2}$$

$$\mu_{l,h} = \mu_{s,h}\left[1 + \frac{1}{Ste(1-t_M)(1+\psi)}\right] \tag{3}$$

$$\mu_{l,c} = \mu_{s,c}\left[1 + \frac{1}{Ste\, t_M (1+\psi)}\right] \tag{4}$$

where L is the length of the bed (m), v_f is the fluid superficial velocity (m/s), and t_M is the dimensionless melting temperature $(\cdot)$ given by $t_M = t(T_M)$ where

$$t(T) = \frac{(T_{i,h} - T)}{(T_{i,h} - T_{i,c})} \tag{5}$$

The accumulation parameter ψ (ratio of the sensible heat of the fluid in the bed to that of the packing) is defined as

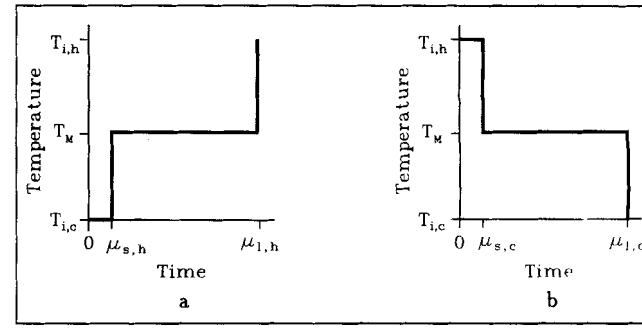

Figure 1. Ideal PCR outlet fluid temperature histories.

(a) Ideal heating period; (b) ideal cooling period. Note $\mu_{l,h}$ and $\mu_{l,c}$ are the dimensionless times required for thermal breakthrough in the respective period.

$$\psi = \frac{\epsilon_B \rho_f C_{p,f}}{(1-\epsilon_B)\rho_p C_{p,p}} \tag{6}$$

where ϵ_B is the bed porosity (m^3 packing/m^3 bed), ρ_f and ρ_p are the densities (kg/m^3) of the fluid and the packing, respectively, $C_{p,f}$ and $C_{p,p}$ are the heat capacities (kJ/kg K) of the fluid and packing, respectively. The Stefan number *Ste* (ratio of PCM sensible heat to latent heat) is defined by

$$Ste = \frac{C_{p,\mathrm{PCM}}(T_{i,h} - T_{i,c})}{\lambda\, \epsilon_{SC}} \tag{7}$$

where $C_{p,\mathrm{PCM}}$ is the heat capacity (kJ/kg·K) of the PCM, λ is the latent heat of the pure phase-change compound (kJ/kg), ϵ_{SC} is the porosity of the PCM support compound (m^3/m^3).

For any process the second-law efficiency η_2 is defined as the ratio of the useful exergy extracted to the total exergy supplied to the process (Szargart et al., 1988). For a heat regenerator, with the ground-state temperature T_0 taken to be equal to the lowest temperature supplied ($T_{i,c}$), the efficiency is given by

$$\eta_2 = \frac{\dot m_c C_{p,c}\int_0^{\theta_c}\left[(T_{o,c}-T_{i,c}) - T_{i,c}\ln\left(\frac{T_{o,c}}{T_{i,c}}\right)\right]d\tau}{\dot m_h C_{p,h}\int_0^{\theta_h}\left[(T_{i,h}-T_{i,c}) - T_{i,c}\ln\left(\frac{T_{i,h}}{T_{i,c}}\right)\right]d\tau + B_{i,c,st} + B_{i,h,st}} \tag{8}$$

where $\dot m_c$ and $\dot m_h$ are the mass flow rates (kg/s) during the cooling and heating periods, respectively, $C_{p,c}$ and $C_{p,h}$ are the mean heat capacities (kJ/kg·K) of the fluid(s) for cooling and heating period, respectively, θ_c and θ_h is the process cycle time (s) for the cooling and heating periods, respectively, τ is the time coordinate (s), $B_{i,c,st}$ and $B_{i,h,st}$ are the strain exergies (kJ), i.e., the work required to pump the fluid during the cooling and heating periods, respectively. Substituting Eqs. 2, 3, and 4 into Eq. 8 and neglecting the exergy terms for moving the process fluid(s) ($B_{i,c,st}$ and $B_{i,h,st}$), one obtains the following expression:

$$\eta_2 = \frac{Ste(1+\psi)\left[(T_{i,h}-T_{i,c}) - T_{i,c}\ln\left(\frac{T_{i,h}}{T_{i,c}}\right)\right]}{\left[Ste(1+\psi)+\frac{T_{i,h}-T_{i,c}}{T_{i,h}-T_M}\right]\left[(T_{i,h}-T_{i,c}) - T_{i,c}\ln\left(\frac{T_{i,h}}{T_{i,c}}\right)\right]} + \frac{\frac{T_{i,h}-T_{i,c}}{T_M-T_{i,c}}\left[(T_M-T_{i,c}) - T_{i,c}\ln\left(\frac{T_M}{T_{i,c}}\right)\right]}{\left[Ste(1+\psi)+\frac{T_{i,h}-T_{i,c}}{T_{i,h}-T_M}\right]\left[(T_{i,h}-T_{i,c}) - T_{i,c}\ln\left(\frac{T_{i,h}}{T_{i,c}}\right)\right]} \tag{9}$$

Consider now the limiting case when $Ste \to 0$ where sensible heat storage can be neglected. In addition, define a nondimensional temperature $\tilde t$ which is referenced to $T_{i,c}$, as

$$\tilde t = \frac{T}{T_{i,c}} \tag{10}$$

Then Eq. 9 becomes

$$\eta_2 = \frac{\frac{\tilde t_{ho}-1}{\tilde t_M - 1}[(\tilde t_M - 1) - \ln \tilde t_M]}{\frac{\tilde t_{ho}-1}{\tilde t_{ho}-\tilde t_M}[(\tilde t_{ho}-1) - \ln \tilde t_{ho}]} \tag{11}$$

where $\tilde t_M$ is the dimensionless melting temperature and $\tilde t_{i,h}$ is the ratio of $T_{i,h}$ to $T_{i,c}$. From this expression one may show (Erk, 1992) for any arbitrary $\tilde t_h$, that η_2 has a maximum in the interval $0 < \tilde t_M < \tilde t_{ho}$. Differentiating Eq. 11 with respect to the ratio $\tilde t_M/\tilde t_{ho}$ and equating to zero yields the expression

$$(\tilde t_M \tilde t_{ho} - \tilde t_{ho})(\tilde t_{ho} - \tilde t_M)(\tilde t_M - 1) - \tilde t_M \tilde t_{ho}(\tilde t_{ho} - 1)(\tilde t_M - 1 - \ln \tilde t_M) = 0 \tag{11a}$$

which, when solved for $\tilde t_M$ gives the optimal melting temperature which maximizes the efficiency. Figure 2 shows a plot of η_2 as a function of the ratio $\tilde t_M/\tilde t_{ho}$ for various values of the

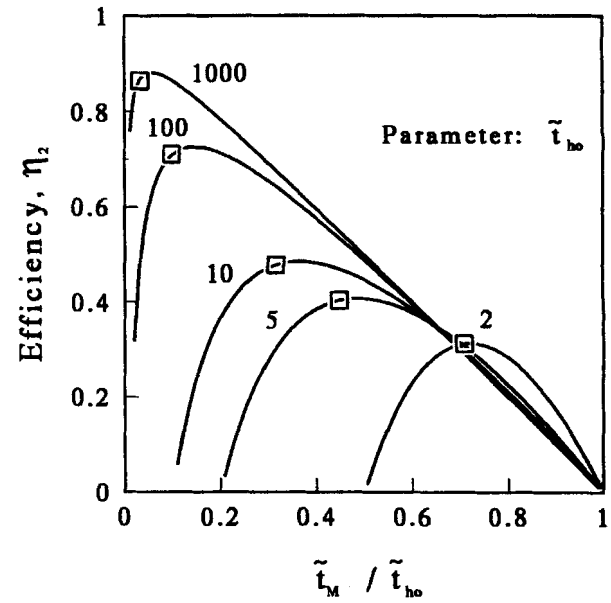

Figure 2. Melting temperature effect on the ideal PCR efficiency.

Rectangles are the predictions $\tilde t_{oh}^{1/2}$ (Lim et al., 1992).

parameter $\tilde{t}_{ho}$. Rectangles on this figure show the prediction $\tilde{t}_M = \tilde{t}_{ho}^{1/2}$ for optimal efficiency, made by Lim et al. (1992). Lim et al. state that this approximation will underpredict the optimal value of efficiency which is confirmed by our analysis. This demonstrates, however, that their approximation is quite good.

PCR: Mathematical Description

Our major objective is to present a model for a PCR using a supported PCM. As mentioned earlier, the model developed should provide information on energy transmission and storage on two scales, the bed scale and the PCM scale. In addition, for the PCM scale, the model should provide information on the position of the melt front within the PCM. This means that a front-tracking formulation must be used to describe the Stefan problem on the PCM scale (Crank, 1984). Note that for the PCM, the Stefan problem applies only when there are two phases. When the PCM is a single phase, the problem reduces to the unsteady Fourier heat conduction equation. On the bed scale, one must account for conduction and convection of heat axially through the bed. Energy storage and transmission on the bed scale can be modeled well using the classical axial dispersion equation (Lai, 1983).

The analytical solution for the coupled set of nonlinear equations, i.e., the axial dispersion model coupled with the Stefan/Fourier problem on the PCM scale, is difficult, if not impossible, to find. The model presented here is based upon a numerical approximation to simultaneously solve the problem for both the particle and the bed scale. Before presenting the model equations in detail, the strategy for obtaining a numerical solution will be presented.

One approach to numerically solving the model equations for the particle (PCM) and/or bed (PCR) scales is to utilize a PDE solver package, such as SIMUSOLV. However, the form and number of equations on the PCM scale changes as the PCM moves from single phase, through two phase and finally back into single phase. Moreover, at different locations in the bed the state of the PCM (whether the PCM is undergoing phase change or not) is different. Upon discretizing the bed, for each location in the bed a separate PCM problem must be solved. Particular attention must be given to the accounting of the PDEs which describe the Stefan problem (two-phase PCM) or the transient Fourier heat conduction problem (single-phase PCM). Furthermore, if one discretizes the PCM scale, all the PDEs describing the model become ODEs which may be integrated by a robust ODE integrator which can handle large systems of stiff ODEs. The first attempts to solve the model equations used this approach: viz. solving a collection of PDEs describing the PCM scale at discrete locations in the bed. Whenever a PCM at a particular location changed from single phase to two phase, or vice versa, i.e., whenever the problem on the PCM scale changed from Stefan to Fourier, or vice versa, the number of equations changed. Therefore, the ODE integrator needed to be restarted using as initial conditions (ICs) the final conditions and temperature profiles of the previous collection of equations. The very large number of stiff ODEs (and the need to frequently restart the ODE integrator) led to excessive demands for computation time.

In an effort to reduce both the complexity of the task and the computation time, a new approach was implemented. This approach is used to solve the model presented here. Basically, the bed is discretized into a collection of heat storage cells. Each cell receives fluid from the cell below it and delivers fluid to the cell above it. The ODEs describing an individual cell are integrated from zero time to a sufficiently long enough time. The outlet temperature-time history is fitted, such as using cubic splines, to a function which can be used as the forcing function for the next cell. Thus, the problem is solved by marching sequentially from the first cell to the last cell, solving the ODEs for only one cell while determining the outlet temperature response and using this as the inlet forcing function for the next cell. When this strategy was implemented, computation time to solve the complete problem was reduced by about three orders of magnitude. Thus, our model is based upon discretizing the bed into cells.

The model equations presented below are based upon the following assumptions:

- No radial temperature gradients on the bed scale.
- No radiation heat transfer on either scale.
- All physical properties are constant.
- The PCM is a sphere.
- The PCM is a supported one, where the physical properties are isotropic and at any point they can be taken as a volume average of the phase change compound and the support matrix.
- Furthermore, the pore size of the support matrix is sufficiently small that there is no melt convection in the liquid phase of the PCM. This includes convection due to density differences between solid and liquid phase change material.
- The PCM is a single phase at the start.

A logical discretization scheme for the axial dispersion equation is to invoke the cells-in-series approximation, which Deans and Lapidus (1960) have shown to be equivalent to a central finite difference approximation of the axial dispersion equation with $N = Pe_a/2$, where N is the number of tanks and Pe_a is the Peclet number for heat transfer

$$Pe_a = \frac{L v_f \rho_f C_{p,f}}{k_{\text{eff}}} \tag{12}$$

where k_{eff} is the effective thermal conductivity of the bed. The approximation is good for long regenerators where the Peclet number is large, but even when Pe_a is small, Deans and Lapidus have pointed out that the nondimensional time coordinate transformation

$$\theta^* = \frac{Pe_a}{2N}\theta \tag{13}$$

where θ the time coordinate and θ^* the transformed coordinate, can be used. Thus, N may be set to a large value to improve the accuracy of the approximation regardless of the value of Pe_a.

Then, the bed is modeled as a collection of N well-mixed tanks (cells) in series. Designate $t_{f,i}$ as the dimensionless temperature, nondimensionalized via Eq. 5, leaving the ith cell. In nondimensional form, the bed scale equation is then

$$\psi \frac{\partial t_{f,n}}{\partial \vartheta} = N(t_{f,n-1} - t_{f,n}) - St(t_{f,n} - t_{\mathrm{PCM}}|_1); \quad 1 \le n \le N \quad (14)$$

where $t_{\mathrm{PCM}}|_1$ represents the temperature at the outer surface of the PCM in the mixing cell, and ϑ is the nondimensional time coordinate which is defined by

$$\vartheta = \psi \frac{v_f}{\epsilon_B L} \tau \quad (15)$$

with τ the actual time. The Stanton number for heat transfer St (ratio of film convection to fluid convection in the bed) is defined as

$$St = \frac{3(1-\epsilon_B)hL}{R_{\mathrm{PCM}} v_f \rho_f C_{p,f}} \quad (16)$$

where h is the convective heat-transfer coefficient (kW/m^2·K) and R_{PCM} is the radius of the PCM (m). The boundary condition at the inlet is

$$t_{f,0} = t_{\mathrm{inlet}} \quad (17)$$

The tanks-in-series representation automatically satisfies the Hulburt boundary condition at the regenerator outlet. For large values of Peclet number, the number of tanks is set to $Pe_a/2$. For small values of Peclet number the time transformation (Eq. 13) may be used. In this case the Stanton number and accumulation parameter must also be transformed using

$$St^* = \frac{St\,2\,N}{Pe_a} \quad (18)$$

$$\psi^* = \frac{\psi\,2\,N}{Pe_a} \quad (19)$$

Then, the equation is the same as Eq. 14 with ϑ, St and ψ replaced by the respective transformed (*) quantities. This indicates that virtually any value of N may be used if the above transformations are invoked.

The tanks-in-series approximation is an integral (energy conserving) approximation, i.e., any errors in the transmission and storage of energy in a cell by using a low value of N should not affect the overall energy balance. It is, therefore, a sensible approximation to use, particularly when one considers the simplification and reduction in computation time afforded by discretizing the axial dispersion and sequentially solving the equations for only one cell at a time.

The classical Stefan problem which is solved on the PCM scale for this situation is given by two PDEs of the form

$$\frac{1}{\varphi^2}\frac{\partial}{\partial \varphi}\left(\varphi^2 \frac{\partial t_y}{\partial \varphi}\right) = \frac{3Bi}{St}\frac{\partial t_y}{\partial \vartheta}; \quad \omega_{x,y,i} < \varphi < \omega_{x,y,o} \quad (20)$$

where φ is the dimensionless radial coordinate in the PCM sphere ranging from 0 at the center to 1 at the outer radius, t_y is the y-phase temperature and Bi is the Biot number for heat transfer, defined as

$$Bi = \frac{hR_{\mathrm{PCM}}}{k_{\mathrm{PCM}}} \quad (21)$$

where k_{PCM} is the effective thermal conductivity of the PCM (kW/m·K). The terms $\omega_{x,y,i}$ and $\omega_{x,y,o}$ are the endpoints (in dimensionless coordinates), where the subscript x is replaced by c in a cooling period and h in a heating period, the subscript y is replaced by s for solid phase and l for liquid phase, and the subscripts i and o represent inner and outer endpoints of the domain. Values of ω are defined as

$$\omega_{h,s,i} = 0 \quad \omega_{h,s,o} = \delta_d \quad \omega_{h,l,i} = \delta_d \quad \omega_{h,l,o} = 1$$
$$\omega_{c,l,i} = 0 \quad \omega_{c,l,o} = \delta_d \quad \omega_{c,s,i} = \delta_d \quad \omega_{c,s,o} = 1$$

where δ_d is the dimensionless position of the solid-liquid interface within the PCM. The boundary conditions (BCs) for the two PDEs are

$$\varphi = 0; \quad \frac{\partial t_{yi}}{\partial \varphi} = 0 \quad (22a)$$

$$\varphi = \delta_d; \quad t_s = t_l = t_M \quad (22b)$$

$$\varphi = 1; \quad \frac{\partial t_{yo}}{\partial \varphi} = Bi(t_f - t_{yo}) \quad (22c)$$

where for a heating period $yi = s$, $yo = l$ and for a cooling period $yi = l$, $yo = s$.

Note

$$t_{\mathrm{PCM}} = t_{yo}|_{\varphi=1}$$

The initial condition (IC) is

$$\vartheta = 0; \quad 0 \le \varphi \le 1; \quad t_{yo} = t_M \quad (23)$$

The position δ_d is given by an energy balance at the solid-liquid interface

$$\frac{\partial t_s}{\partial \varphi} - \frac{\partial t_l}{\partial \varphi} = \frac{3}{St}\frac{Bi}{Ste}\frac{\rho_{\mathrm{PC}}}{\rho_{\mathrm{PCM}}}\frac{d\delta_d}{d\vartheta}; \quad \varphi = \delta_d \quad (24)$$

We next consider how the Stefan problem should be discretized. Due to the spherical geometry, the solution to the Stefan problem is nonlinear in position as δ_d approaches the center of the PCM. For example, Figure 3 shows the temperature profile in the PCM at several times. As the solid-liquid interface nears the center, the temperature in the liquid shell surrounding the solid core rises very sharply. Attempts to approximate these profiles using low-order polynomials are not fruitful because these profiles really have a $1/r$ dependence due to the spherical geometry. Indeed, analytical solutions to classical problems involving this geometry are often solved by transforming into one of linear flow (Carslaw and Jaeger, 1959) (i.e., into slab coordinates). For this problem this is done

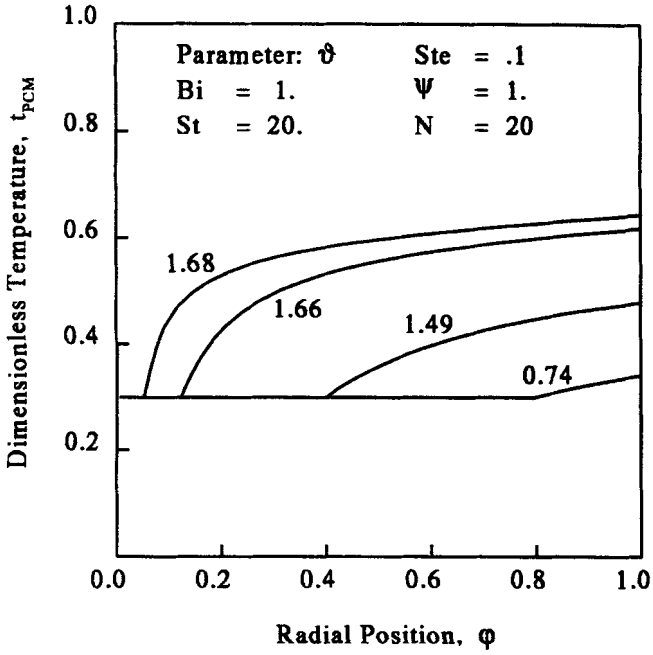

Figure 3. Temperature profiles in a PCM during a heating period.

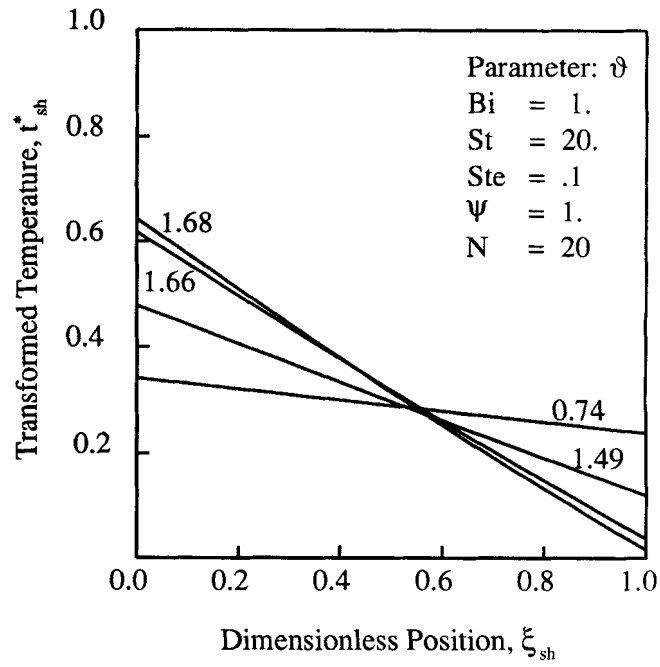

Figure 4. Effective slab temperature profiles in the shell-phase PCM.

by defining a transformed temperature in the shell surrounding the core

$$t^s_{sh} = \varphi t_{sh} \tag{25}$$

where the subscript *sh* designates this for the shell phase (liquid during a heating period and solid during a cooling period). Note that the core phase need not be transformed since the boundary conditions force the solution to be smooth and easily approximated by low-order polynomials. Thus, a numerical solution should contain the transformation described in Eq. 25 for the shell phase.

Besides the nonlinearity of the shell-phase temperature profile, another difficulty with numerically solving the Stefan problem is the fact that the domain of each of the two PDEs changes over time. Numerically, it is more efficient to immobilize the boundary (Crank, 1984). We define the immobilized coordinate system for the core and shell phases respectively ξ_{co} and ξ_{sh} each of which span [0, 1] by

$$\xi_{co} = \frac{\varphi}{\delta_d} \tag{26a}$$

$$\xi_{sh} = \frac{\varphi - 1}{\delta_d - 1} \tag{26b}$$

By first transforming the temperature profile in the shell phase and immobilizing the boundary, the profile becomes approximately linear. For example, Figure 4 shows the transformed, immobilized shell phase temperature profiles for the same times and parameters given in Figure 3. Low-order polynomial trial functions easily and accurately approximate these curves.

The PDEs of the Stefan problem are converted into a series of ODEs by discretization of the spatial coordinates. Orthogonal collocation (Villadsen and Michelson, 1978; Finlayson, 1972) is used. The collocation coefficients using symmetric trial functions in spherical geometry (defined here as $A_{j,i}$ and $B_{j,i}$ for $i, j = 1, \ldots, P_{cs}+1$) are used for the core phase since the BC at the center is automatically satisfied. The collocation coefficients using nonsymmetric trial functions in slab geometry (defined here as $D_{j,i}$ and $E_{j,i}$ for $i, j = 0, \ldots, P_{cu}+1$) are used for the shell phase with the temperature transformed using Eq. 25. Thus, the Stefan problem becomes the following set of $P_{cs} + P_{cu} + 1$ ordinary differential equations (ODEs)

$$\frac{dt_{co,j}}{d\vartheta} = \frac{St}{3\,Bi\,\delta_d^2} \sum_{i=1}^{P_{cs}+1} B_{j,i} t_{co,i} + \frac{1}{\delta_d}\frac{d\delta_d}{d\vartheta} \sum_{i=1}^{P_{cs}+1} A_{j,i} t_{co,i} \xi_{co,i}; \quad \text{for } j = 1, \ldots, P_{cs} \tag{27a}$$

$$\frac{dt^s_{sh,j}}{d\vartheta} = \frac{St}{3\,Bi\,(\delta_d - 1)^2} \sum_{i=0}^{P_{cu}+1} D_{j,i} t^s_{sh,i} + \frac{1}{(\delta_d - 1)}\frac{d\delta_d}{d\vartheta} \sum_{i=0}^{P_{cu}+1} E_{j,i} t^s_{sh,i} \xi^s_{sh,i}; \quad \text{for } j = 1, \ldots, P_{cu} \tag{27b}$$

$$\frac{d\delta_d}{d\vartheta} = \frac{St\,Ste\,\beta}{3\,Bi\,\gamma_{co}\,\delta_d} \left(\sum_{i=1}^{P_{cs}+1} A_{P_{cs}+1,i} t_{co,i} + t_{sh}|_{t=t_M} - \frac{1}{\delta_d - 1} \sum_{i=0}^{P_{cu}+1} D_{P_{cu}+1,i} t^s_{sh,i} \right) \tag{27c}$$

where β is $+1$ for a heating period, and -1 for a cooling period, and γ_{co} is the ratio of the core-phase density at the PCM melting point to the reference density. The boundary condition at the PCM surface is a nonlinear equation

$$Bi(t_{f,n} - t_{sh,0}) = -t^s_{sh,0} + \frac{1}{\delta_d - 1} \sum_{i=0}^{P_{cu}+1} D_{0,i} t^s_{sh,i} \quad (28a)$$

and the BC at the moving interface is

$$t_{co,P_{cs}+1} = t_{sh,P_{cu}+1} = \frac{t^s_{sh}}{\delta_d} = t_M \quad (28b)$$

When the PCM is not undergoing phase change, the collocation approximation for the unsteady Fourier conduction equation can be used; this equation is the same as that given for the core phase of the Stefan problem. In this case, the boundary condition at the surface of the PCM is given by the following linear equation

$$Bi(t_{f,n} - t_{PCM,0}) = \sum_{i=1}^{P_{cs}+1} A_{1,i} t_{PCM,i} \quad (28c)$$

Then one must solve only P_{cs} ODEs for the PCM scale.

The complete model is thus solved numerically by integrating in time for each of the N stages in the regenerator the ODEs which are described by Eq. 14, Eqs. 27a, 27b, and 27c, as well as by associated boundary and initial conditions. Each stage is solved independently, starting from $\vartheta = 0$ to the ending time. Then, the next cell is solved, thereby marching cell by cell along the regenerator. The output from a cell is stored in an array and cubic splines are used to approximate the temperature history so that it could be used as input for the next mixing cell. The routine **TAUTSP** (de Boor, 1978) was used to approximate the temperature history. The ODEs were integrated using the **LSODES** integrator which utilizes the ODEpack integrator package (Hindmarsh, 1983). Solving the model cell by cell has the advantage of minimizing the number of ODEs which must be solved. For each cell $P_{cs}+1$ ODEs are integrated when the PCM is a single phase, and $P_{cs} + P_{cu} + 1$ ODEs are integrated when the PCM is changing phase. With a minimal number of ODE to be integrated, the speed and accuracy of solving the problem is maximized, particularly in light of the fact that the ODEs are stiff, particularly at the onset and end of phase change.

Changing from a two-phase problem to a single-phase problem is readily accomplished. The profile which is estimated for the shell phase at the instant that $\delta_d = 0$ (within a specified tolerance) is interpolated into the spherical coordinates of the single-phase sphere for the Fourier problem, resetting the ICs, changing the number of ODEs to be integrated, and restarting the integrator.

Performing the opposite task, i.e., going from a single-phase problem to a two-phase problem, is not so easy. The front-tracking ODE, Eq. 27c contains a $\delta_d - 1$ term. This equation is indeterminate for $\delta_d = 1$. The equations must be started by some other method. The approach taken here was to use Neuman's analytical solution for a slab with constant heat flux at the surface (Carslaw and Jaeger, 1959). This solution is valid for the PCM sphere if the melt front δ_d has moved only a small distance inward, and the time taken to do this is very small. Neuman's solution is expressed in terms of a double power series in space and time. Further details on this solution are given elsewhere (Erk, 1992).

A computer program was written to implement the solution algorithm which has been presented. The program was written in standard Fortran 77, and has been ported to the Washington University Chemical Engineering Apollo DN 4500 workstation running unix (f77 compiler) and an IBM compatible 486 (Microway NDP 386/486 compiler and Lahey F77L-EM/32 compiler). It requires less than 2 Mb of core memory to execute. Run times vary from several hours on the workstation, to less than 30 min on the 486 PC. It was found that the collocation order need not be larger than five to give accurate results, as verified by the overall energy balance. This means that no more than six to twelve ODEs were integrated, and this number is independent of the number of stages used in the TIS approximation. The program output gives detailed stage-by-stage summary of the calculation history, the histories of fluid temperature, PCM center temperature, PCM surface temperature, and δ_d for each stage. A total energy balance calculation is also performed as a check on the accuracy.

Simulation Results

Energy balance

The energy balance for the PCR is given by

$$\text{energy stored or released} = 1 + \psi + \frac{1}{Ste}$$

When only sensible heat is involved (i.e., the unit is operated in a temperature range which does not include the melting point of the PCM) the third term containing *Ste* is dropped. Table 1 compares the computed energy balance against the theoretical value when only sensible heat storage occurs. The energy balance for both the heating period and the cooling period is exact to three digits of precision. The program yields an energy balance which deviates from the actual value by at most one-quarter of a percent.

The energy balances for PCR simulations (phase change does occur within the bed) are presented in Table 2. The error is generally below one-quarter of a percent, with a maximum error of one-half of a percent. The energy balance error is the largest when the PCR response is sluggish, and for large times ($\vartheta > 40$). The error is due to large time steps, selected by the **LSODES** integrator. Reducing the step size improves the energy balance, but at the expense of computation time.

Table 1. Energy Balances for PCR Simulations with Sensible Heat Storage Only*

Bi	*St*	ψ	Calc. Energy Stored	$1+\psi$	% Error
5.0	10.0	1.000	1.999	2.000	0.05
5.0	10.0	0.001	1.002	1.001	−0.10
0.1	1.0	1.000	1.998	2.000	0.11
0.1	1.0	0.001	1.003	1.001	−0.24

*Other parameters: $N = 20$; $t_M = 1.1$; $Ste = 0.1$.

Table 2. Energy Balances for PCR Simulations with Phase-Change Heat Storage*

Bi	*St*	ψ	Calc. Energy Stored	$1+\psi$ $+1/Ste$	% Error
1.0	10.0	1.000	11.994	12.000	0.05
10.0	10.0	0.001	11.002	11.001	−0.01
10.0	10.0	0.010	11.011	11.010	−0.01
10.0	10.0	0.100	11.100	11.100	−0.00
10.0	10.0	1.000	12.000	12.000	−0.00
10.0	10.0	5.000	16.000	16.000	−0.00
10.0	10.0	10.000	20.999	21.000	0.00
0.1	10.0	1.000	11.940	12.000	0.50
25.0	10.0	1.000	12.003	12.000	−0.22
50.0	10.0	1.000	11.935	12.000	−0.53
10.0	50.0	1.000	11.999	12.000	0.00
10.0	20.0	1.000	12.000	12.000	0.00
10.0	5.0	1.000	12.001	12.000	−0.01

*Other parameters: $N = 20$, $t_M = 0.3$, $Ste = 0.1$.

Parametric studies

The effect of the parameters t_M, ψ, *Ste*, *St*, and *Bi* were investigated.

Effect of t_M. To maximize efficiency, the optimal melting temperature is given by Figure 2 or Eq. 1. In dimensionless form, assuming $T_0 = T_{i,c}$, this means that t_M is approximately 0.5 for low temperature ranges ($T_{i,h} - T_{i,c} < 10$) to 0.7 for high temperature ranges ($T_{i,h} - T_{i,c} \approx 1{,}300$). Examining Eqs. 2 through 4, one observes that as the melting temperature of the PCM changes, the length of time required for thermal breakthrough changes. For low values of t_M, the heating period breakthrough time is shortened, while for high values the cooling period breakthrough time is shortened. Figure 5 shows this effect. As the PCR becomes more nonideal, the length of the constant temperature zone is also reduced (see Figure 6). However, there always is some zone, albeit small in duration (length), where the response moves through a temperature t_M. When this zone becomes sufficiently small, it represents an inflection point in the response. Of course, when this happens, the PCR is not operating efficiently in the sense of the second law.

The reader may observe the presence of wiggles in Figure 5. At first, one may suspect these wiggles are an indication that the numerical method is having difficulty and the results may be suspect. Actually, the wiggles are an indication that the number of cells used to approximate the axial dispersion equation N is small. It can be shown (Erk, 1992) that there are always exactly $N-1$ wiggles and that they are generated in each cell when latent-heat energy storage terminates in the cells below. As N increases, the magnitude of the wiggles decreases. One may observe this on later figures where $N = 50$ is used instead of the value of $N = 20$ used in Figure 5. It must be emphasized, however, that despite the presence of these wiggles, the overall energy balance is still satisfied due to the conservative nature of the tanks-in-series approximation. The real temperature response is simply a smoothed response of what is shown in Figure 5. Hence, passing a smooth line through the wiggles would be justified, but not done here. Most importantly, the effect of t_M is completely unaffected by this artifact. Further details may be found in Erk (1992).

Effect of ψ. The accumulation parameter is the ratio of the volumetric heat capacity of the fluid to that of the PCM. The value of ψ is $\mathcal{O}(10^{-3})$ when the fluid passing through the PCR is a gas and $\mathcal{O}(1)$ when the fluid is a liquid. From the definition of ψ, it is apparent that ψ should affect the fluid temperature history by changing the velocity of the temperature front through the bed, as shown for the ideal PCR in Eqs. 2, 3 and 4. The effect should only be seen at larger values of ψ, i.e., for liquid working fluids and to a much greater extent for the first front than for the second. The velocity of the first front is proportional to the inverse of $1+\psi$. The velocity of the second front is proportional to $1+\psi+$

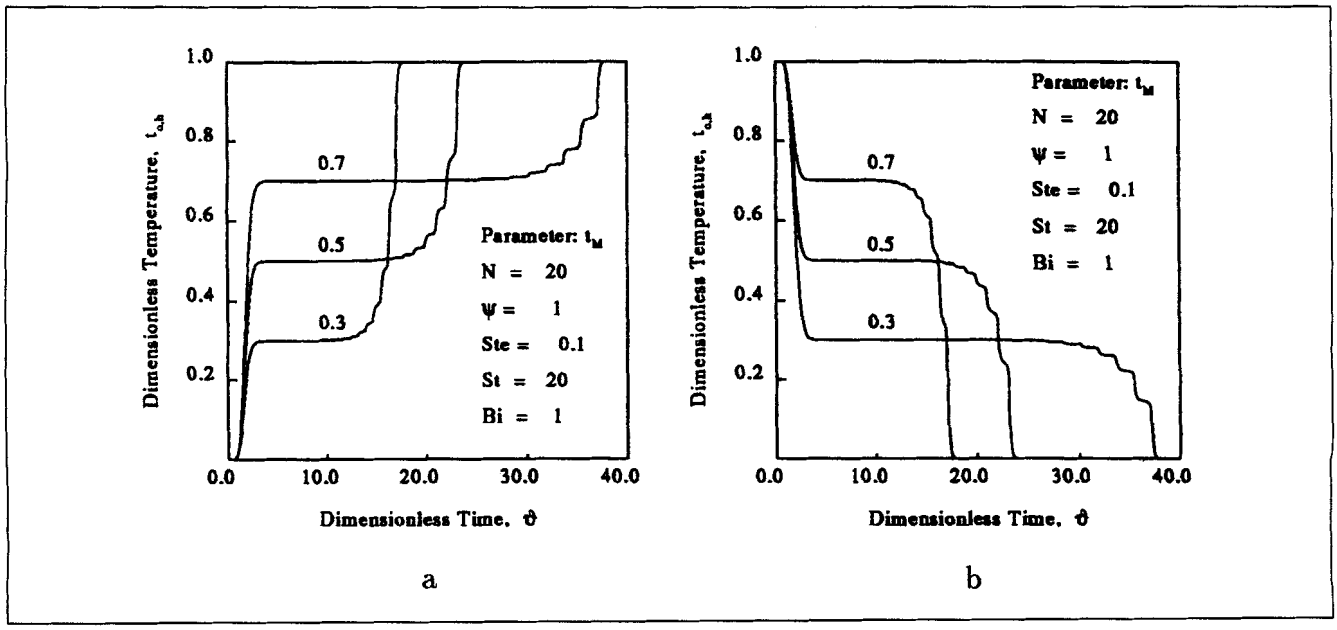

Figure 5. Effect of t_M on the fluid temperature history.

(a) Heating period; (b) cooling period.

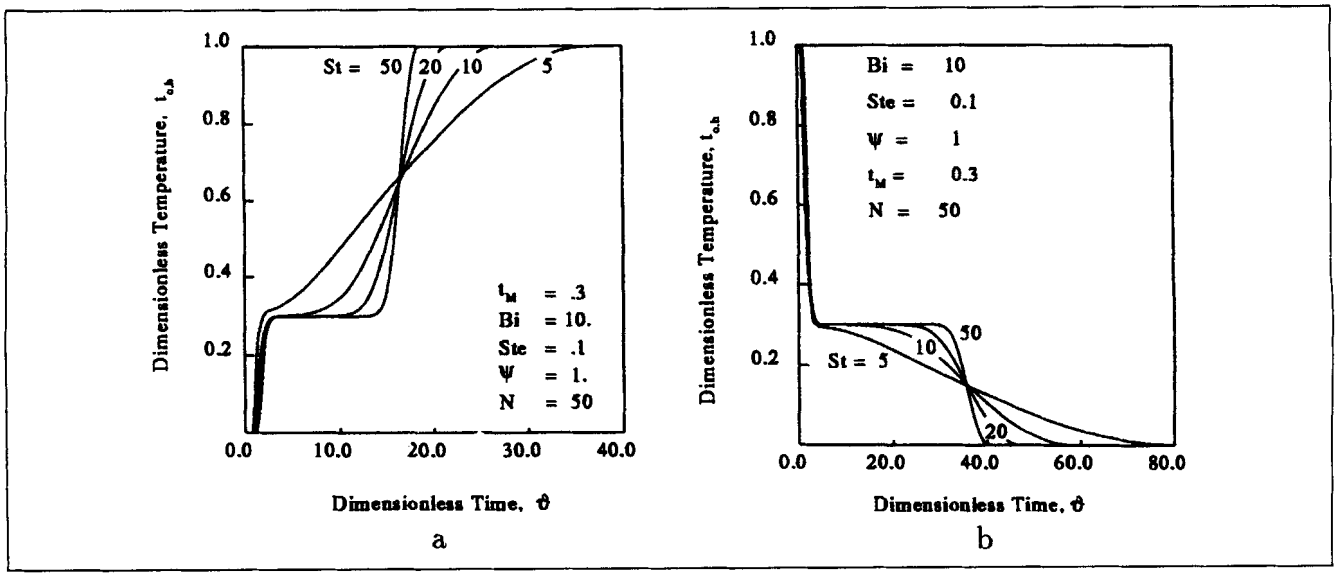

Figure 6. Effect of *St* on the fluid temperature history.

(a) Heating period; (b) cooling period.

latent heat contribution. The latent heat contribution is significantly larger than ψ. Figures 4.10a and 4.10b presented by Erk (1992) show this effect. They are not reproduced here in the interest of brevity. Essentially, the shape of the temperature response remains unchanged with different values of ψ, since the effect of latent heat dictates the overall shape of this response. However as ψ increases, the entire response curve is shifted forward to longer times, since the onset of the response is governed by the passage of the first front (the sensible-heat front) through the bed.

Effect of Ste. The Stefan number is the ratio of sensible heat to latent heat of the PCM. When $Ste \rightarrow \infty$ sensible heat storage dominates, while when $Ste \rightarrow 0$ latent heat storage dominates. For optimal PCR operation, the latter limiting case is preferred, since this means that there is a great amount of latent heat which can be stored (relative to sensible heat). However, physical properties of useful phase-change compounds and usable temperature ranges generally limit *Ste* to $\mathcal{O}(10^{-2})$. The practical upper limit on *Ste* is $\mathcal{O}(1)$, since larger values of *Ste* would mean that the amount of latent heat which can be stored is less than the amount of sensible heat. The reciprocal of *Ste* is a measure of the length of the zone where $t_{o,x} = t_M$ for the ideal PCR. This effect is shown in Figures 4.11a and 4.11b presented by Erk (1992). Since the PCR shown in these figures is not ideal, decreasing *Ste* not only lengthens the constant-temperature zone, but also lengths the transition zone between two-phase and single-phase heat storage modes, near the end of the period.

Effect of St. The Stanton number is defined as the ratio of interphase heat transfer by film convection to intraphase heat transfer by bulk-flow convection. It is a gauge of the relative importance of convection on each of the length scales. Generally *St* ranges between 0.5 and 300, depending upon the working-fluid phase, the physical properties, and the fluid flow rate through the bed. As $St \rightarrow \infty$, the PCR becomes more ideal, since the characteristic time for heat transfer by bulk convection is much greater than the characteristic time for heat transfer by film convection around the PCM. The effect of *St* can be seen in Figure 6, which shows a series of responses (with *St* as the parameter) for the heating period (Figure 6a) and the cooling period (Figure 6b). For a value of *St* of 50, the PCR performance is close to ideal, while for a value of 5 the performance is very nonideal. For the nonideal PCR the outlet temperature is greater than t_M for a heating period and less than t_M in a cooling period, since the energy in the fluid cannot be transferred to/from the PCM fast enough.

Effect of Bi. The Biot number is defined as the ratio of heat-transfer rate by convection in the film surrounding the PCM to the heat-transfer rate by conduction in the PCM. Generally, *Bi* can range between 0.1 and 100 depending upon the value of the convective heat-transfer coefficient. As *Bi* increases, the rate of heat supply to the PCM increases. When this happens, the rate of heat supply to the PCM is greater than the rate of heat conduction in the PCM, so heat cannot be stored at a fast enough rate. Figure 7 shows this effect of *Bi* upon the temperature response. As *Bi* decreases from 50 to 0.1, the response begins to resemble that of the ideal PCR. This effect is evident in both the heating period, Figure 7a, and the cooling period, Figure 7b.

From Eq. 20, one observes that rather than the Biot number itself, a more meaningful measure of the nonideality of the PCR caused by PCM thermal conduction is the ratio of the *Bi* and *St*. The term $(3\,Bi/St)$ is the ratio of heat transfer by bulk convection in the bed to heat transfer by conduction in the PCM. So, as the characteristic time for heat transfer in the PCM becomes smaller relative to the characteristic time for heat convection along the bed, the PCR becomes more efficient at storing heat and thereby approaches the ideal PCR. Thus, as $(3\,Bi/St) \rightarrow 0$ the PCR becomes more ideal.

Bed scale fronts

Our model can also be used to look inside the PCR bed and visualize temperature fronts. Figure 8 shows the temperature profile as it moves in time through the PCR. The pa-

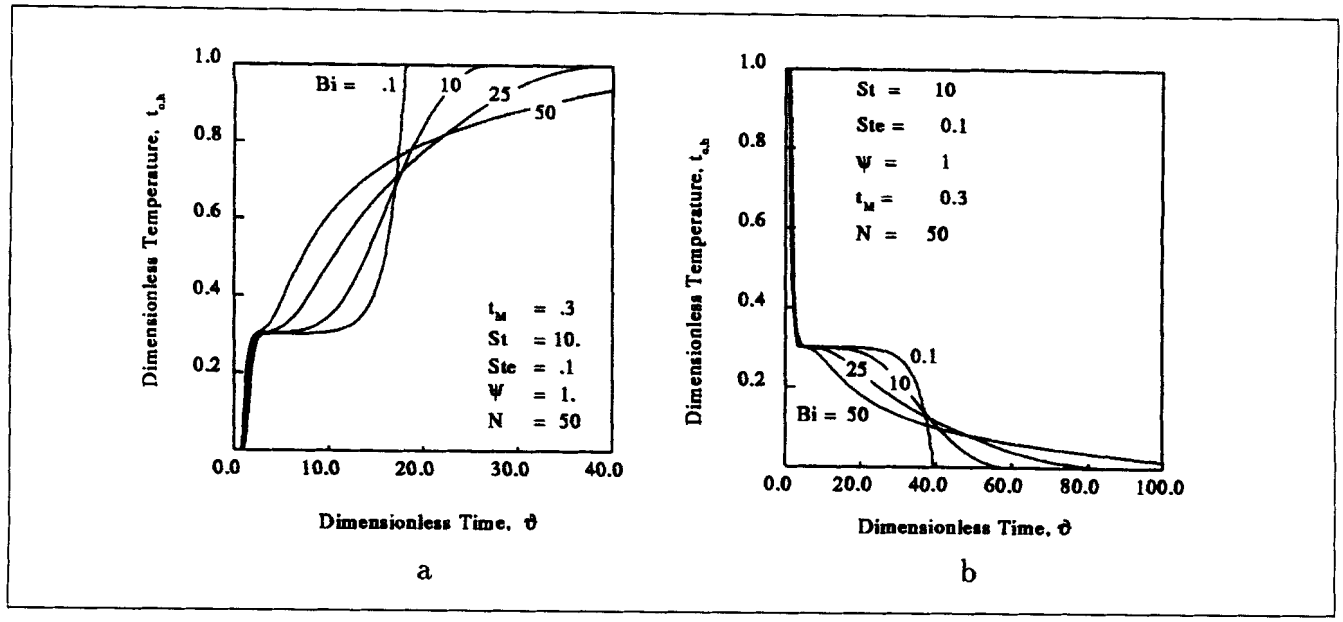

Figure 7. Effect of *Bi* on the fluid temperature history.

(a) Heating period; (b) cooling period.

rameters were selected so the response is close to that for the ideal PCR. The temperature profiles have the same shape and move through the bed in the same fashion as described earlier for the ideal PCR.

Figure 9 shows the temperature profiles for the conventional regenerator which may be compared with those shown in Figure 8a, for the nearly ideal PCR. For short times, the profiles of the two regenerators are similar. Once the latent heat effect is felt, however, the two-step temperature profile begins to form.

In addition to the temperature steps which move through the bed, another type of front moves through the bed. There is a zone of PCM which is undergoing phase change centered between two zones of PCM which are not undergoing phase change. There are two moving fronts: the two boundaries between the three zones. Although δ_d is a quantity related to the PCM-sphere scale, it can be linked to the bed scale through the coupling of the model equations. A δ_d of either 1 or 0 in a given mixing cell indicates the PCM in that mixing cell is not undergoing phase change. Alternatively, if the PCM in a mixing cell has a δ_d which is between 0 and 1, then there is a phase change occurring in this cell, *ipso facto*. At the beginning of the simulation, δ_d for each cell is initialized to 1. After the PCM has finished undergoing phase change the

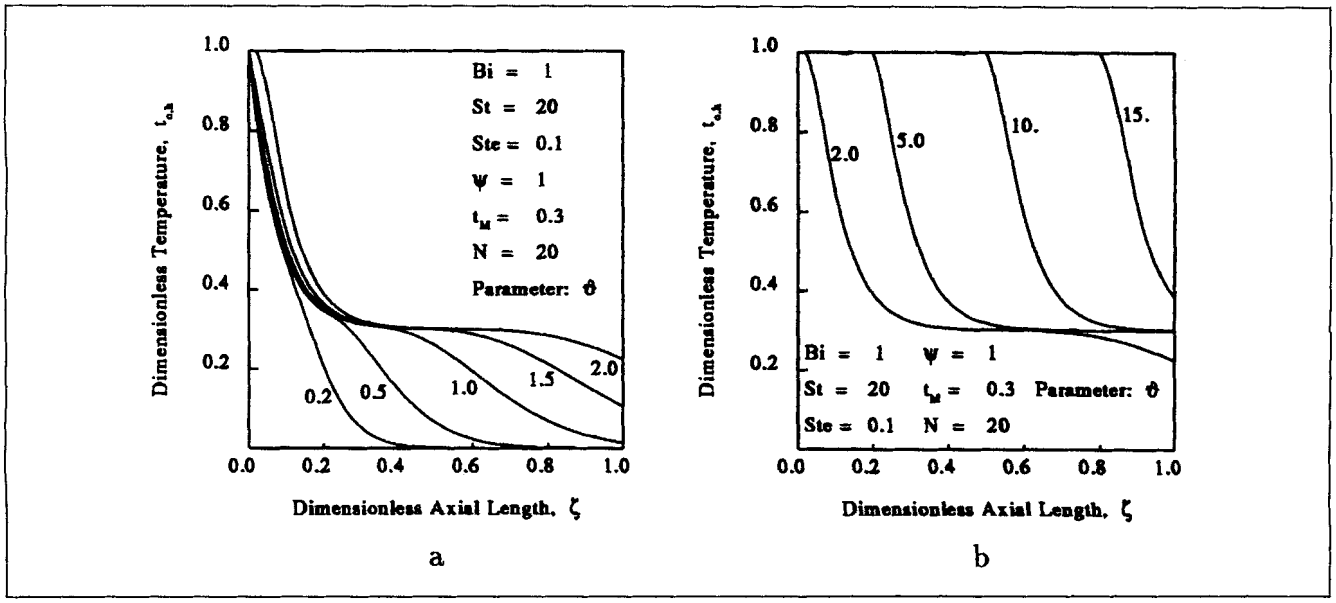

Figure 8. Heating period temperature profiles in the PCR.

(a) Short times; (b) long times.

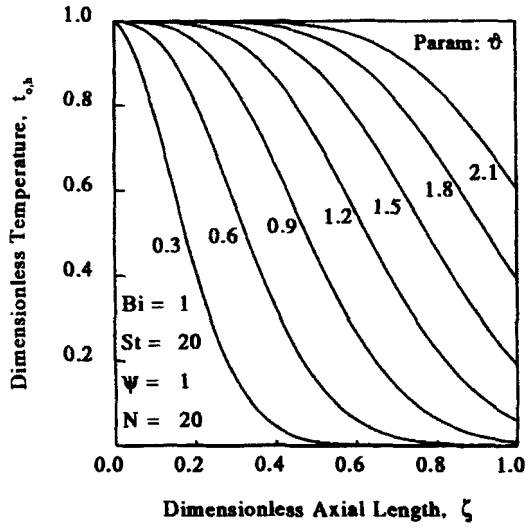

Figure 9. Axial temperature profiles in the PCR.

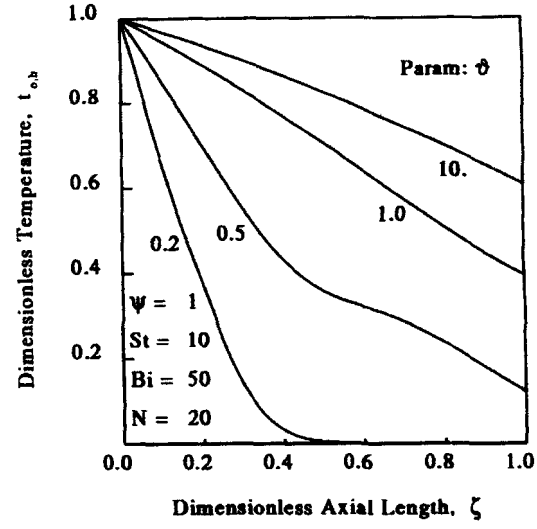

Figure 11. Axial temperature profiles in a nonideal PCR.

value remains 0. Thus by plotting the value of δ_d for each cell, the zones of PCM undergoing phase change can be seen. Figure 10 shows a plot of a profile of δ_d as it moves through the bed in time. About 20% of the bed is undergoing phase change.

The profiles presented so far have been for a PCR which is close to ideal. When the PCR is quite nonideal, the temperature profiles resemble the conventional regenerator, although the profile movement is much slower. Figure 11 shows a set of temperature profiles at different times for such a nonideal PCR. For this regenerator, the entire bed is undergoing a slow phase change as illustrated by the axial profiles of δ_d shown in Figure 12.

Another method of visualizing temperature movement through the regenerator is by using a thermogram. These are plots where regions of color or gray level are mapped to the temperature. Post-processing programs were written to input the stage history files generated by the model and general color PostScript output to visualize the temperature profile in the PCR. Then, the PostScript code can be converted into a variety of graphic formats which allow rendering into an animated visualization program. This visualization allows the observer to conduct a simulated PCR experiment and view the temperature movement through the bed. These animations can be viewed on a 80386 PC with SVGA graphics. In addition, there is software which would allow animations in these formats to be viewed on unix-based systems under the X Window System. Further details on this, and sample thermogram can be found elsewhere (Erk, 1992).

PCR Experiments

An experimental, lab-scale, low-temperature PCR was built to test the model. Only a brief description of the test PCM and PCR will be presented here. Complete details and dimensional drawings of all subcomponents of the apparatus are given elsewhere (Erk, 1992).

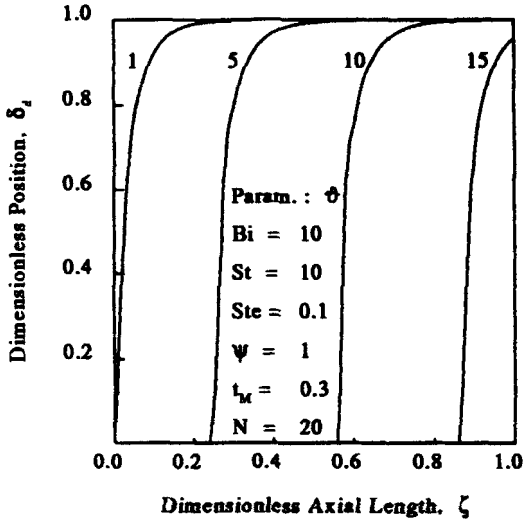

Figure 10. Axial δ_d profiles in the PCR.

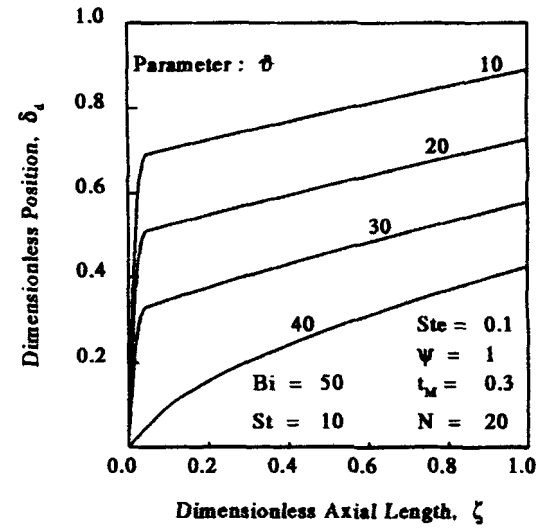

Figure 12. Axial δ_d profiles in a nonideal PCR.

Experimental studies

Experimental PCM. A supported PCM was made by filling high porosity silica catalyst carriers with *n*-octadecane wax. This wax melts at room temperature, has a relatively high latent heat of fusion, and can be obtained at relatively high purity. Shell International Chemical Company, Ltd. manufactures a silica catalyst support with a very small pore diameter (v. de Jongste, 1984). These spheres are easily filled with liquid wax, which is drawn into the small pores and held there by capillary force. During the course of development, it was discovered that the pore size of the silica support is critical. If it is too small, the *n*-octadecane molecular motion is hindered, thereby adversely affecting latent heat storage capacity (Erk, 1992). If the pores are too large, there is insufficient capillary force to retain the liquid wax. The support used for this research was S980G 1.5, with a diameter of 1.5×10^{-3} m, and a mean pore size of 60×10^{-9} m. This PCM is opaque, white when the wax is solid, but turns transparent, when the wax is liquid. Thus, the PCM has the advantage that the solid/liquid melt front can be visually tracked (both within the bed and within the PCM itself if one looks closely enough). The PCM was characterized by a variety of techniques, including differential scanning calorimetry (DSC). Physical properties are given in Table 3.

Experimental PCR. Figure 13 shows a flow diagram for the experimental PCR. The experimental apparatus consisted of a thermal-conditioning system which allowed the working fluid to be heated or cooled to a fixed, steady temperature; a well-insulated, but transparent bed through which the front could be visualized; and a data acquisition system for collecting time/temperature data at the inlet and outlet of the bed.

The thermal-conditioning system consisted of two heat exchangers, each immersed in separate constant-temperature baths, Haake NK22, item 10 in Figure 13, which have both heating and cooling. The bath temperature control capability is within ±0.2°C.

The heat exchangers, item 9 in Figure 13, were made from 1/2-in. (13-mm)-OD soft-wall copper tube (3/8 L soft tubing) which were filled with -3 $+14$ copper shot (Aldrich catalog number 22,340-9) and coiled around a 0.127-m-dia. mandrel mounted in an engine lathe chuck. The tubes were filled with shot prior to coiling. The tube compressed as it formed so that the wall of the tube was pressed tightly against the shot providing good thermal contact.

In addition to the heat exchanger, a wax saturator, item 8 in Figure 13, was placed in the bath as well. Although *n*-octadecane wax has a low vapor pressure ($<10^{-3}$ m of mercury) it will be carried away by the gas stream, so a saturator was added to each bath to minimize PCR wax inventory loss. The saturator was built from copper pipe. After installing the saturator and the heat exchanger in the constant-temperature bath, the piping was insulated.

Table 3. Physical Properties of Experimental PCM

Property	Symbol	Value	Unit
Latent Heat of Fusion	λ_{PCM}	90.0	kJ/kg
Melting Point	t_M	25.8	°C
Solid Density	ρ_{PCM}	1,234.6	kg/m^3
Solid Thermal Conductivity	k_{eff}	0.45	W/m·K
Solid Specific Heat	$C_{p,PCM}$	1.36	kJ/kg·K
Diameter	d_{PCM}	1.51	10^{-3} m

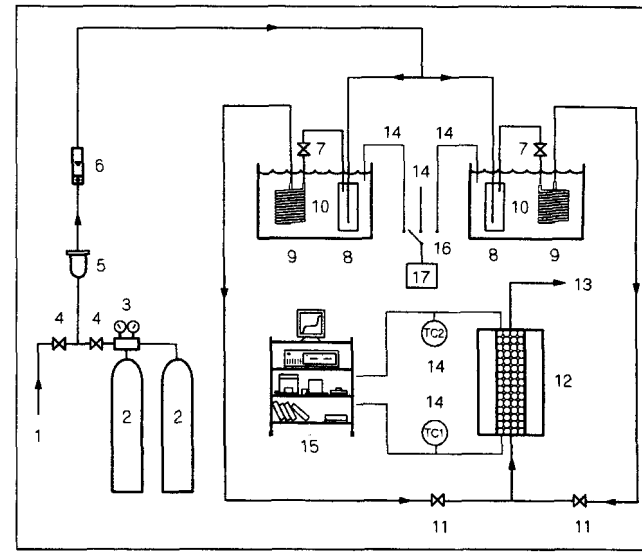

Figure 13. Experimental PCR.

(1) Compressed air; (2) gas cylinder; (3) regulator; (4) gas-select valve; (5) filter; (6) rotameter; (7) bath isolation valve; (8) wax saturator; (9) coil heat exchanger; (10) temperature bath; (11) PCR isolation valve; (12) PCR; (13) to fume hood; (14) T thermocouple; (15) data acquisition system; (16) thermocouple switch; and (17) temperature indicator.

Since carbon dioxide has a relatively high heat capacity, is relatively inexpensive and easy to handle, it was selected as the working fluid. Commercial grade CO_2 supplied in cylinders, item 2 in Figure 13, was used. To conserve the gas used in the experiments, a separate compressed air line was added. In this fashion the system could be thermally equilibrated with air rather than CO_2. During the experiment, gas from one of two cylinders, item 2, flows through a heated regulator and into a gas rotameter, item 6. The gas splits into two streams, one for each bath, entering the saturators. From the saturators, the gas flows through the heat exchanger. From the heat exchanger, the gas flows to a 1/4 in. NPT PVC stopcock valve, item 11. From this point to the PCR, the piping is insulated polypropylene tubing.

The PCR consisted of a thin-walled, clear bed container which is surrounded by a vacuum jacket to minimize heat losses. The bed container is a clear polycarbonate tube 35×10^{-3}-m ID with a 1.6×10^{-3}-m wall and 0.318 m long. A transparent measuring scale, ruled in 0.5×10^{-3}-m increments, was affixed to the outside of the bed container. Care was taken to assure the rule was placed parallel to the axis of the tube. After mounting to the bed container tube, the graduations on the rule were checked against a precision scale and found to be correct to within 0.5×10^{-3} m over the entire length.

The PCM is confined in the tube by two porous distributor plates at the ends of the tube. These distributor plates, 6×10^{-3} m thick, were made from porous polypropylene, 0.15×10^{-3} m average pore size. A fine-gauge Type-T thermocouple (Omega COCO-001) with a junction bead diameter of approximately 7×10^{-5} m was suspended in a 6×10^{-4} m wide groove cut into the inner surface of the distributor plate. The thermocouple leads are sealed to the outer surface of the porous plate. Each distributor disk is held in an O-ring sealed holder, machined from PVC which slips snugly into the bed

container tube. The distributor plate holder has a threaded port through which the CO_2 can flow and through which the thermocouple leads can be connected with a gas-tight feedthrough.

The bed container tube, filled with PCM and capped at both ends with the thermocouple-embedded distributor plates, was centered in the vacuum-jacket containment tube (thick-walled, 7.6×10^{-2} m ID, transparent, acrylic tube). The ends of the vacuum jacket tube were sealed with PVC disks which had O-ring seals. The jacket was continuously pumped. In this fashion, pressure was exerted on the ends of the PCR to maintain a gas-tight seal between the CO_2 in the bed and the vacuum surrounding the bed. To more readily track and measure the melt front, two mirrors were installed in the vacuum jacket. The mirrors aided in minimizing parallax errors in reading the melt front position.

Data Acquisition. Temperature measurements from the inlet and outlet of the PCR were recorded by a simple data acquisition system consisting of a genuine IBM PC with an eight-bit Data Translation DT 2801 A/D board installed. Thermocouple emf was converted to a 0 to 10 VDC signal with an Analog Devices 3B01 signal conditioning system, with two 3B47-T-07 type-T thermocouple modules installed, and fed into the DT 2801 through a Data Translation terminal panel, model DT 707. After assembly and checkout, the 3B47 modules were calibrated with an Omega model CL23 calibrator to give optimal accuracy in the temperature range of 15 to 40°C. Maximum error was within 0.5°C in this temperature range.

A simple data acquisition program was written to record the two raw temperature signals from the PCR and 3B47s, and convert to temperature values. The program acquired data at a user-input time interval and recorded both the raw signal and the calculated temperature for both the temperature inputs on the hard disk.

Results

Two types of data were gathered from the experiments: (1) Melt or solidification front movement in the bed; (2) CO_2 outlet (and inlet) temperature history.

The front movement in the bed had to be visually recorded, while the data acquisition system automatically recorded the temperature histories. Front movement data consisted of recording an average front position as a function of time. The average was based on reading two positions. The mirrors placed in the PCR allowed one to read the melt front on the left and right sides of the bed near the mirrors. Using this technique, the results were reproducible and independent of the bias of the observer. It was generally much easier to visualize the heating period front movement, since the transition from opaque to transparent in the PCM was easily seen. During a cooling period, however, since the wax melted from the outside and moved inward, the transition was from transparent to milky and finally opaque was not as easily detected. On careful examination, one could discern the movement of the two fronts (the sensible heat and the latent heat fronts) as was described earlier for the ideal PCR. For both heating and cooling periods, the fronts began fairly flat and became more nonuniform as the front moved through the bed. Towards the end of the bed, the nonuniformity became as large as 1.5×10^{-2} m, or about 5% of the overall length of the bed.

Table 4. Values of Dimensionless Groups for PCR Experiments*

Flow Rate	80%	70%	60%	40%
Bi	0.16	0.14	0.13	0.10
N	275	240	205	140
Pe	550	480	410	280
St	140	150	160	170
Ste**	0.2	0.2	0.2	0.2
t_M^***	0.58	0.58	0.58	0.58
ψ	0.00054	0.00054	0.00054	0.00054
ϑ/τ‡	0.0025	0.0023	0.0020	0.0013

*Value in column heading is flow meter reading as percent of full scale. Maximum value is 80%.
**Nominal value. Actual value depends upon experiment.
‡Not a dimensionless group, but used to nondimensionalize time. Dimensions: s^{-1}.

Photographs showing this behavior as a function of time are shown elsewhere (Erk, 1992).

The experiments were performed in sets of two: first a heating period, followed by a cooling period. A total of 24 experiments were performed. When slightly more than half of these experiments were finished, the bed was repacked. The thermal response, at the same conditions, for the two different bed packings reproduced within 10% of each other. Table 4 lists the values of the dimensionless groups which were explored in the course of experimentation.

Figure 14a shows the gas inlet and outlet temperatures for a typical heating period experiment. The response shown in Figure 14a resembles that expected for a typical PCR as described earlier. Figure 15a shows the melt front movement through the bed. The front moves through the bed at a relatively constant velocity for more than half the cycle and then as the front nears the end of the bed, the velocity falls off.

Figure 14b shows the gas inlet and outlet temperatures for a typical cooling period. In contrast to the general PCR described earlier, there are two phase-change steps. Figure 15b shows the solidification front movement through the bed. There is more variability of the front velocity.

Both Figures 14a and 14b show a nonideality which impacts markedly the performance of the PCR, viz. the lack of a sharp step in the inlet temperature response. In both heating and cooling periods the inlet response does not attain its steady-state value until approximately 1,500 s, or approximately 15% of the period duration. This sluggish response is due to two factors: first, the thermal mass of the distributor plate and associated piping and second, the heat losses primarily through the distributor plate assemblies at the ends of the regenerator. As will be discussed in the following section, the first factor may be accounted for by modifying the inlet forcing function of the PCR model; however, the second factor is not accounted for and leads to a discrepancy between model prediction and PCR performance.

Discussion

The nonuniformity of the front shape which is observed is most likely due to nonuniform wax distribution in the PCM. In some areas of the packing, when the wax is a liquid, there was excess wax on the outside of the PCM, while in other areas the support may not have been fully saturated with wax. When the wax solidifies, it is drawn inward because of the

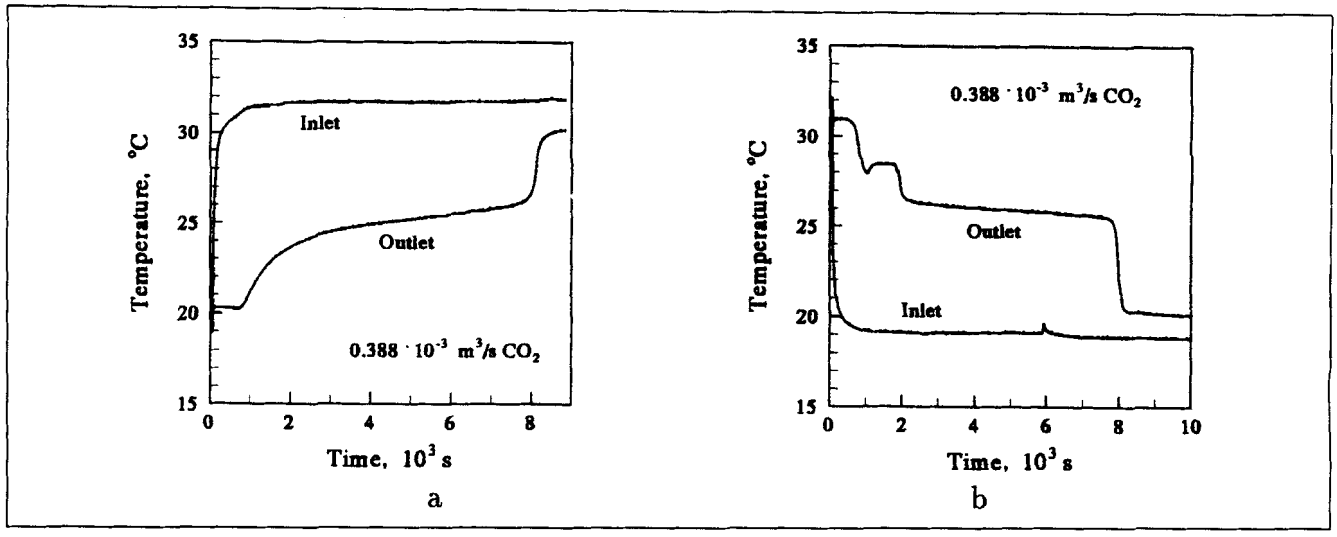

Figure 14. Gas temperature histories for a heating and a cooling period.

(a) Heating period; (b) cooling period.

density change of *n*-octadecane. This nonuniform distribution of wax causes small temperature gradients within the bed, since the pure wax on the outside of the PCM freezes at a different temperature (and has a different latent heat) than the wax which is supported within the pores of the PCM. This has been verified experimentally by the DSC characterization described earlier. The wax molecules which are adsorbed on the pore walls of the support do not have as free a mobility as they would outside the pore. Thus, the support behaves as in impurity in the wax, depressing the freezing point and latent heat. The classical Van't Hoff expression

$$\Delta T_M = \frac{RT_M^2 x}{MW\lambda_{PC}}$$

may be used to predict, within less than 5% error, the freezing point depression (Erk, 1992). This is why one observes two steps in the cooling period curve shown in Figure 14b. The first step, at approximately 28°C, is due to pure *n*-octadecane (not held in the pores of the support) freezing. The second step, at 26°C, is due to the wax within the PCM freezing. In the first phase-change step (that of the pure wax) one can also observe a small supercooling effect. Supercooling was not observed in any of the experiments for the wax supported by the PCM itself. Figure 14b can be thought of as a thermal chromatogram which separates, in temperature, the heat-storing components of the PCR. The dual step is not observed in the heating period because there is no excess wax on the outside of the PCM after the *n*-octadecane has solidified.

Because of this complexity, which was not accounted for in the model, it was not attempted to fit the model to cooling period data. However, a fit of the model to a heating period was made. A simulation, using the program discussed earlier, was performed for the experiment shown in Figure 14a. Fig-

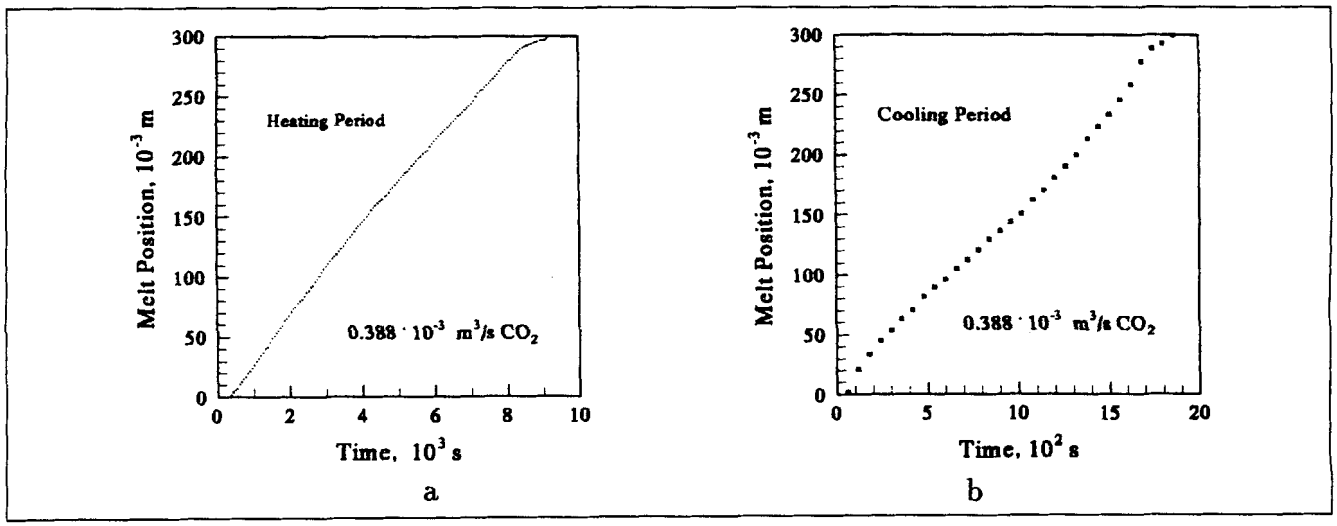

Figure 15. Melt front position history for a heating and a cooling period.

(a) Heating period; (b) cooling period.

ure 16a shows a comparison between experiment and model prediction. The model appears to agree qualitatively with the experiment, but predicts sharp transitions in temperature which are not evident in the data. This comparison is, however, somewhat misleading because the temperature recorded at the outlet of the bed is affected by heat losses from the bed, namely from the top distributor plate. When energy balances were made using the experimental data, the total energy removed from the CO_2 was 37 kJ, while the energy stored by the PCM in the bed was only 24 kJ. This discrepancy was consistent for all heating period experiments. Furthermore, for cooling period experiments the discrepancy was reversed, such as when 37 kJ of energy was transferred to CO_2 while the PCR only released 24 kJ of energy. Heat losses account for over 50% of the energy inventory in the bed. This loss is primarily through the ends of the regenerator. Early on in data analysis, some steady-state temperature measurements indicated that fluctuations in ambient room temperature were detected as temperature fluctuations at the ends of the bed. Incidentally, one may also hypothesize that some CO_2 may have been leaking into the vacuum jacket, thereby introducing an error. It is unlikely the leak was significant, however, because several times during the course of experimentation the pump which maintained the vacuum jacket was isolated and the vacuum in the jacket was maintained.

Additional evidence that the dominant effect is due to heat losses at the end of the bed is seen if one compares the front position data with model predictions. Figure 16b shows this comparison. Note that this comparison uses the same simulation results which were employed to generate the poor fit of outlet temperatures shown in Figure 16a. The fit between the model and the experimental data is very good up to about 60% of the bed (0.18×10^{-3} m). After this point, the experimentally-measured front movement slows and near the end (within the last 10^{-2} m) slows even more. A heat loss would explain the slowing of the front and the deviation from the model prediction. Note that Figure 15b, the front position for a cooling period, shows the melt front movement slowing in speed as the front nears the end of the bed. Heat transfer to/from the bed tube is responsible for the initial deviation of the front from the model. Near the end of the experiment the heat loss by heat transfer to/from the distributor plate affects the melt front movement, and this is responsible for the hooking which is evident in Figures 15a, 15b and 16b. This observation is further evidence for the contention that temperature measurements at the outlet of the PCR are smeared by heat loss to the distributor plate. As mentioned in the previous section, the effect of heat losses at the inlet end of the PCR can be seen as a smeared inlet temperature response.

To illustrate how significant these effects are, an approximate model for the distributor plate can be formulated. Consider a section of the plate, the thickness of the depth of the slot in which the thermocouple is suspended. The equation describing, approximately, this bed is given by

$$\frac{dt_f}{d\vartheta} = A_1(t_{o,p} - t_f) - A_2(t_f - t_{dp})$$

where if this were part of the regenerator bed, A_1 would be $1/\psi$ and A_2 would be St/ψ, and t_{dp} would be the temperature of the distributor plate. We approximate t_{dp}, using Newton's Law of Cooling, by $t_{o,p}\,[1-\exp(-\vartheta/A_3)]$. Let A_1, A_2 and A_3 be arbitrary. Figure 17 compares the results of Figure 14a against the simulated response with the above equation used to smear the true simulated response. Values of the dimensionless parameters A_1 to A_3 are 0.7, 0.7, and 6.0, respectively, and were chosen to fit the experimental data. The two curves compare well, considering the highly approximate treatment of the end plate effect.

We do not mean to suggest that this empirical treatment is an exact accounting for the heat losses which occurred during the experiments. Indeed, the heat loss of the bed tube is still

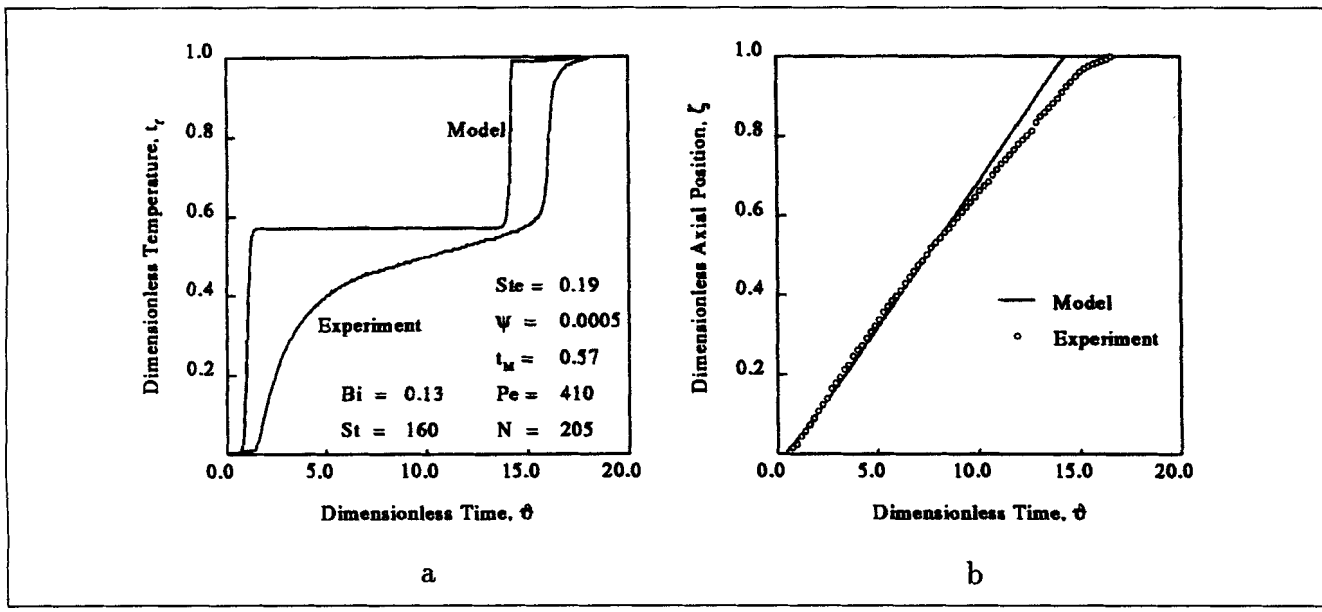

Figure 16. Experiment vs. model predictions.

(a) Gas outlet temperature history; (b) melt front position.

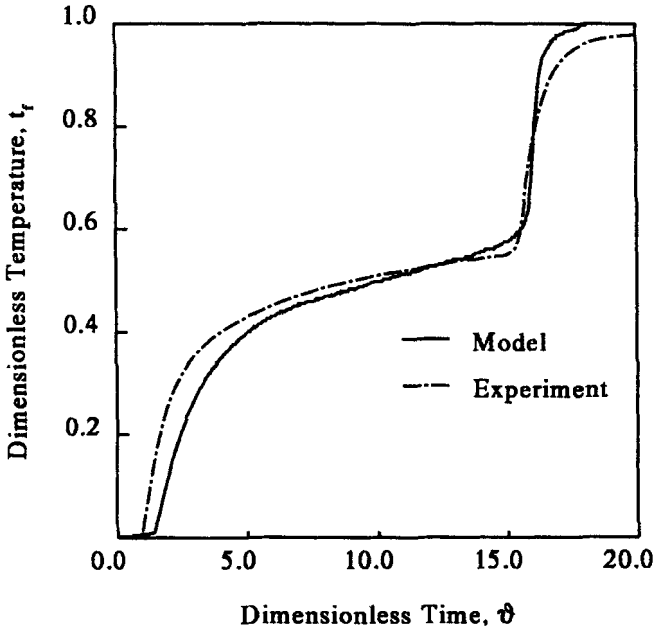

Figure 17. Experiment vs. model predictions: modified outlet temperature history.

Stirred tank at outlet simulates distributor plate heating.

not accounted for. This treatment does suggest, however, that heat losses at the distributor plate, as well as the thermal mass of the distributor plate, can add lags to the response of the thermocouple, thereby invalidating any comparison which can be made between the model and the experiments. More detailed instrumentation is necessary to ascertain quantitatively where energy is being lost. This was beyond the scope of the present work. Nevertheless, it can be argued that sufficient evidence is presented to suggest that the model developed in this study could be used to sufficiently predict the performance of larger, truly adiabatic beds in which end effects and heat losses are negligible relative to the total energy inventory within the bed.

Concluding Remarks

With the importance of heat-recovery technology to reduce energy consumption, there is a need to develop an understanding for the PCR operation. Previous work reported in the literature has shown a need for developing both a detailed model and for comparing this model to experimental data.

The ideal PCR can be thought of as a two-step process, as opposed to the single-step process for the ideal conventional regenerator. Two temperature fronts, separated by a zone at the melting temperature of the PCM, move through the bed, each traveling at a different velocity. The velocity of the first front is equivalent to the velocity for the single temperature front of the ideal conventional regenerator. The velocity of the second front is much slower, due to energy storage by latent heat. Using the ideal PCR model, a second-law thermodynamic analysis predicts that the optimal PCM melting temperature is consistent with the results reported by Lim et al. (1992).

We have presented a computational scheme for the prediction of temperature histories and phase-change front position, solving a model which discretizes the bed into a set of well-stirred mixing cells to model axial dispersion. The PCM scale is modeled successfully by appropriate transformations, immobilizing the moving boundary and discretizing via orthogonal collocation. The numerical solution of the model equations is done efficiently and accurately with minimal computer resources and time. Simulations can be used to predict temperature profiles within the bed and the outlet fluid temperatures. Energy balances are closed to less than 1% in all cases. Parametric studies have verified that for all practical purposes, the ideal PCR is approached for: $(3\,Bi)/St < 5\times10^{-3}$; $Pe > 40$, $St > 50$; $Ste < 10^{-1}$; and $\psi \geq 1$.

The computational model which was developed is comprehensive and robust. It is capable of assessing the effect of operating and design parameters and performance of commercial-size PCRs.

Comparisons made between the outlet fluid temperature which was measured experimentally to that predicted by the model indicate that, in the small insulated bench-scale apparatus, there is a significant amount of heat loss. As much as 50% of the energy stored in the experimental unit can be lost to the surroundings via the end plates. The model prediction of the overall shape of the outlet temperature history compares qualitatively well with PCR experiments. Heat absorption and losses from the ends of the bed and from the bed wall itself are responsible for the discrepancy between experimental results and the model. The model prediction of melt front movement compares quantitatively very well with experimental results for over half the front travel through the bed. Past approximately 60% of the bed, the experimentally measured front movement slows relative to the model predictions. The effect of heat absorption by the bed containing tube explains this deviation. Heat absorption and losses by the porous distributor plate at the outlet appears to be responsible for discrepancies as the front nears breakthrough.

Because of the particular type of PCM which was used in the experiments, there appear to be two different phase-change components, one of pure *n*-octadecane wax and one of the wax which is held in the pores of the support. The pure wax displays a slight supercooling effect which has not been accounted for in the model. Further refinements to the model should include accounting for this supercooling, accounting for multiple phase-change components, and heat losses through the ends of the bed. As it stands, the model, solved by the developed numerical algorithm, is a useful tool for predicting thermal response for large-scale adiabatic PCRs.

Acknowledgments

This project was partially financially supported by The Chemical Reaction Engineering Laboratory of Washington University, and partially from MEMC Electronic Materials, Inc. Some of the PCR experiments were executed by Dr. Jhi Zhou and Mr. Jaieman Gou. Their efforts in diligently collecting the data are appreciated.

Notation

$A_{j,i}$ = first derivative symmetric collocation coefficient (Eq. 27a)
B = exergy, kJ

$B_{j,i}$ = second derivative symmetric collocation coefficient (Eq. 27a)
$D_{j,i}$ = first derivative nonsymmetric collocation coefficient (Eq. 27a)
$E_{j,i}$ = second derivative nonsymmetric collocation coefficient (Eq. 27a)
i, j = collocation coefficient indices (Eq. 27a)
k = thermal conductivity, kW/m·K
n = stage number
P_{cs} = number of symmetric collocation points
P_{cu} = number of nonsymmetric collocation points
Pe = Peclet number for heat transfer (Eq. 12)

Greek letters

β = flux sign correction (Eq. 27c)
γ_{co} = density ratio (Eq. 27c)
δ = dimensionless melt front coordinate (Eq. 22b)
θ = regenerator period, s
μ = temperature breakthrough time (Eq. 2)
ξ = dimensionless immobilized coordinate (Eqs. 26a and 26b)
ω = domain endpoint (Eq. 20)

Subscripts

a = axial
B = bed
co = core phase
f = fluid
i = inlet
o = outlet [first]; outer [third]
PCM = PCM (effective) property
Sh = shell phase
x = generic for h and c
y = generic for s and l
yi = generic for inner phase s or l
yo = generic for outer phase s or l
0 = initial state

Superscripts

id = ideal
$*$ = modified

Acronyms

ADE = axial dispersion equation
ODE = ordinary differential equation
PC = phase-change component
PDE = partial differential equation

Literature Cited

Adebiyi, G. A., "Development of PCM Packed Bed Thermal Model for Industrial Applications," *Proc. Diurnal/Industrial Thermal Energy Storage Research Activities Review* (Mar. 9–10, 1988).

Arimilli, R. V., and A. G. Graves, "Single-Phase Liquid Flow through a Packed Bed of PCM," *Advanced Energy Systems — Their Role in Our Future, Proc. Intersociety Energy Conversion Eng. Conf.*, Amer. Nucl. Soc., Vol. 2, Paper No. 849479, p. 1195 (Aug. 19–24, 1984).

Arimilli, R. V., "Modeling of Transient Heat Transfer in Packed Beds," *Proc. U.S. DOE Thermal Energy Storage Program Review: Report to Industry* (Mar. 11–12, 1987).

Bell, M. A., R. R. Cohen, B. J. W. Manley, P. W. O'Callaghan, and R. J. Wood, "The Development of and Optimisation of Cost Effective Thermal Energy Storage Systems of Solar Space Heating by Means of a Microprocessor Controlled Test Facility," *Proc. EC Contractors' Meeting*, p. 324, D. Reidel Publishing, Dordrecht, Holland (June 14–16, 1982).

de Boor, C., *A Practical Guide to Splines*, Springer-Verlag, New York, p. 299 (1978).

Carslaw, H. S., and J. C. Jaeger, *Conduction of Heat in Solids*, 2nd ed., Chap. XI, pp. 30, 240, Oxford Univ. Press, London (1959).

Chen, S. L., and J. S. Yue, "A Simplified Analysis for Cold Storage in Porous Capsules with Solidification," *Trans. ASME J. Energy Res. Technol.*, **113**, 108 (1991).

Crank J., *Free and Moving Boundary Problem*, Chaps. 3–6, Clarendon Press, Oxford (1984).

Deans, H. A., and L. Lapidus, "A Computational Model for Predicting and Correlating the Behavior of Fixed-Bed Reactors: I. Derivation of Models for Nonreacting Systems," *AIChE J.*, **6**, 656 (1960).

Duduković, M. P., and P. A. Ramachandran, "Heat Regenerators, Design and Evaluation of," *Encyclopedia of Chemical Processing and Design*, Marcel Dekker, New York, p. 390 (1987).

Electric Power Research Institute, *Commercial Cool Storage Design Guide*, Chap. 2, Hemisphere Publishing, New York (1987).

Erk, H. F., "Phase-Change Heat Regenerators: Modeling and Experimental Studies," DSc Thesis, Washington Univ., St. Louis, MO (Dec., 1992).

Fellague, A. A., and L. F. Jesch, "Solar Space Heating and Phase Change Energy Storage," *Proc. Int. Conf. on Energy Options — The Role of Alternatives in the World Energy Scene*, IEE, The Chameleon Press, London, p. 66 (Apr. 7–9, 1987).

Finlayson, B. A., *The Method of Weighted Residuals and Variational Principles*, Academic Press, New York, p. 96 (1972).

Graves, A. G., "Transient Thermal Performance of an Experimental Packed Bed Thermal Energy Storage System," MS Thesis, Univ. of Tennessee, Knoxville (June, 1985).

Hausen, H., *Heat Transfer in Counterflow, Parallel Flow and Cross Flow*, translated from German by M. S. Sayer, A. J. Willmott, ed., Chaps. 11–19, McGraw-Hill, New York (1983).

Hindmarsh, A. C., "ODEpack, A Systematized Collection of ODE Solvers," *Scientific Computing: Proc. IMACS World Cong. on Systems, Simulation & Scientific Computation, Tenth*, Montreal, W. F. Ames and R. S. Stepleman, eds., Elsevier, North-Holland, Amsterdam, p. 55 (1983).

de Jongste, H. C., "Shell Silica Spheres," *Spec. Chem.*, **41**(2), 42 (1984).

Lai, S., "Periodic Operation of Heat Regenerators: A New Method for Calculation of Thermal Efficiency," MSc Thesis, Washington Univ., St. Louis, MO (Aug., 1983).

Lim, J. S., A. Bejan, and J. H. Kim, "Thermodynamic Optimization of Phase-Change Energy Storage using Two or More Materials," *Trans. ASME J. Energy Res. Technol.*, **144**, 84 (1992).

Manley, B. J. W., and I. E. Smith, "Thermal Energy Storage using Encapsulated Phase Change Materials," *BHRA Fluid Engineering Int. Conf. on Energy Storage: Energy Storage for Energy Management*, BHRA Fluid Engineering, Cranfield, Bedford, U.K. (May 25–26, 1983).

Reay, D. A., *Heat Recovery Systems — A Directory of Equipment and Techniques*, Halsted Press, New York (1979).

Reiter, S., *Industrial and Commercial Heat Recovery Systems*, Chap. 4, Van Nostrand Reinhold, Cincinnati (1983).

Schatz, O., "Cold Start Improvement with a Heat Store," SAE Technical Paper No. 910305, SAE Int. Cong. and Exposition, Detroit (Feb. 25–Mar. 1, 1991).

Schmidt, F. W., and A. J. Willmott, *Thermal Energy Storage and Regeneration*, Hemisphere, New York (1981).

Shamsundar, N., and E. M. Sparrow, "Analysis of Multidimensional Conduction Phase Change Via the Enthalpy Model," *J. Heat Transf.*, **97**, 333 (1975).

Szargut, J., D. R. Morris, and F. R. Steward, *Exergy Analysis of Thermal, Chemical, and Metallurgical Processes*, Hemisphere, New York (1988).

Villadsen, J., and M. L. Michelsen, *Solution of Differential Equation Models by Polynomial Approximation*, Chaps. 3–4 and 8–9, Prentice-Hall, Englewood Cliffs, NJ (1978).

Wood, R. J., S. D. Gladwell, P. W. O'Callaghan, and S. D. Probert, "Low Temperature Thermal Energy Storage using Packed Beds of Encapsulated Phase-Change Materials," *Int. Conf. on Energy Storage*, Vol. 1, BHRA Fluid Engineering, Bedford, U.K., p. 145 (1981).

Manuscript received Feb. 13, 1995, and revision received May 11, 1995.